Water participation in catalysis revealed: an atomistic approach to solvent effects in the catalytic isomerization of allylic alcohols.

Franco Scalambra[1], Nicole Holzmann[2], Leonardo Bernasconi[2], Silvia Imberti[3], Antonio Romerosa[1*]

[1]Área de Química Inorgánica-CIESOL, Universidad de Almería, Almería, Spain. [2]Scientific Computing Department, STFC Rutherford Appleton Laboratory, Harwell Oxford, Didcot, OX11 0QX, UK. [3]ISIS Neutron and Muon Source, STFC Rutherford Appleton Laboratory, Harwell Oxford, Didcot, OX11 0QX, UK.

KEYWORDS: Catalytic isomerization, allylic alcohols, ruthenium complexes, water, neutrons, EPSR, DFT, AIMD, reaction mechanism.

ABSTRACT: We describe the intermediate of the reaction between a ruthenium complex and the 1-propen-3-ol in water by an atomistic approach for gaining information about the conformation and dynamics of complex molecules in aqueous solution, which combines DFT based *ab initio* molecular dynamics (AIMD) and neutron scattering data based on Empirical Potential Structure Refinement (EPSR) simulations. We apply our method to the study of the water soluble η^2-allylic complex $[RuCp(exo\text{-}\eta^2\text{-}CH_2{=}CH\text{-}CH_2\text{-}OH)(PTA)_2]^+$ (**2**) (PTA = 1,3,5-triaza-7-phosphaadamantane), a significant intermediate in the isomerisation of 1-propen-3-ol into propanal catalysed by $\{RuCp(H_2O\text{-}\kappa O)(PTA)_2\}^+$. We identify the factors responsible for the stabilisation of a specific conformer of **2** in water solution and, for the first time, we demonstrate the direct involvement of water molecules in the formation of this species. In particular, we show that long-lived (*ca.* 10 ps) bonded chains of water molecules play a crucial role in influencing the conformation and, potentially, the chemical reactivity of **2**.

1. INTRODUCTION

Carbonyl compounds play a central role in several synthetic and industrial chemistry processes. They can be obtained through several synthetic routes, of which the catalytic redox-isomerization of allylic alcohols mediated by metal complexes (Scheme 1)[1–4] is one of the most atom-efficient (100% conversion) and mechanistically intriguing.

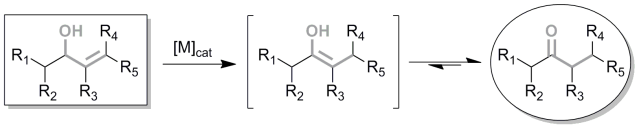

Scheme 1. Metal catalysed isomerization of allylic alcohols.

The metal-catalysed isomerization of allylic alcohols in water solution is particularly attractive, especially under mild reaction conditions, as water displays several advantages in the chemical industry over competing organic solvents, including abundance, price, availability, stability, and minimal environmental impact. Water is however of typically limited use in homogeneous and metal-complex mediated catalysis, largely because most reactive metal-based organometallic complexes are insoluble in water or decompose easily.

As part of our activity during the last years, we have presented complexes possessing antiproliferative activity,[5–7] technologically important optical properties,[8] and catalytic activity,[9–11] including the ability to catalyse the isomerization of allylic alcohols under mild conditions in water.[12] The activity of the catalytic species responsible for the isomerization of linear allylic alcohols $[RuCp(H_2O\text{-}\kappa O)(PTA)_2](CF_3SO_3)$ (**1·CF_3SO_3**)[13] (Scheme 2) is strongly influenced by the presence of water in the reaction (PTA = 1,3,5-triaza-7-phosphaadamantane).

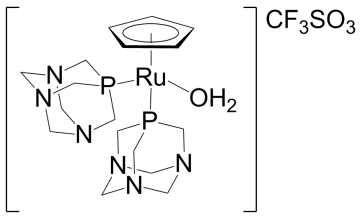

Scheme 2. Structure of **1·CF_3SO_3**.

Furthermore, it has been found that a much higher than stoichiometric amount of water in the reaction medium increases its efficiency significantly.[14] Theoretical studies

have been used to substantiate the involvement of water in catalytic processes akin to the allylic alcohol isomerisation.[15–17] Only a very small number of water molecules were however explicitly taken into account in these studies. The processes through which water molecules assist the catalytic reaction, particularly by stabilising specific reactive conformers in solution, remain largely obscure. In principle, water molecules not only can stabilize reaction intermediates, but they can also potentially modify their electronic structure and reactivity. Developing robust and general procedures to examine the origin of these interactions is therefore of crucial importance for the optimisation of chemical processes in which water plays a central role.

For the specific case of metal catalysed isomerization of allyl acohols[15,18] three main mechanisms have been proposed in the literature (Scheme 3): a) the metal hydride addition-elimination mechanism, also named alkyl mechanism; b) the π-allyl metal hydride or η^3-allyl mechanism; c) a mechanism invoking oxygen coordination, also known as enone mechanism.[19] Preliminary experimental results on the conversion of linear allylic alcohols by **1** indicated that mechanism b) is the most probable.[14] The observed dependence of the conversion rate on the amount of water is however not accounted for by this mechanism.

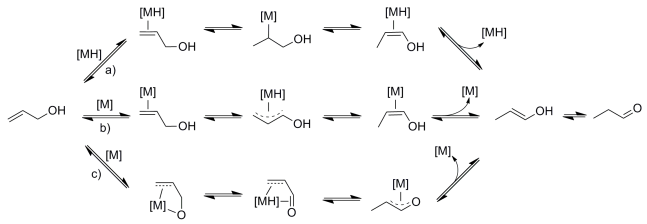

Scheme 3. Proposed mechanisms for the catalytic isomerisation of allyl alcohols: a) alkyl mechanism; b) η^3-allyl mechanism; c) enone mechanism.

We have shown in previous studies on the parent complex $[RuCp(PTA)_2\text{-}\mu\text{-}CN\text{-}^1\kappa C{:}^2\kappa^2 N\text{-}RuCp(PTA)_2](CF_3SO_3)$ that water molecules interact not only with N_{PTA} atoms, but also with the Cp moiety.[20] Therefore, the interaction of **1** with water molecules can occur through the metal atom, the ancillary ligands, the substrate and/or the N_{PTA} atoms. All of these interactions can influence the reaction outcome. In this work we present a combined study of NMR measurements, AIMD simulations, neutron scattering experiments and EPSR simulations of the isolated intermediate complex (**2**·CF_3SO_3) obtained by reaction of **1**·CF_3SO_3 with 1-propen-3-ol, which is the simplest linear allylic alcohol. The aim of this study is to apply this combination of experimental and computational techniques to gain insight into the nature of water-solute interactions and to unveil specific features in the solvation environment, which contribute to the stabilisation of the reactive species **2** in solution.

2. RESULTS AND DISCUSSION

2.1 Catalytic isomerization of 1-propen-3-ol mediated by 1-CF_3SO_3: synthesis and characterization of 2·CF_3SO_3. The catalytic isomerisation of 1-propen-3-ol into propanal in the presence of **1**·CF_3SO_3 in water, MeOH or 1-propen-3-ol is highly inefficient (<0.2 %) at room temperature. At 80 °C the catalytic conversion occurs in water (ca. 12% conversion), but not in MeOH or 1-propen-3-ol (ca. 1 %). It is important to observe that one water molecule is always present, as a ligand, in the structure of

Figure 1. ^{1}H-^{1}H NOESY NMR of **2** in D_2O. Assignment of the hydrogens of the allylic ligand and structures of the *exo* and *endo*-isomers.

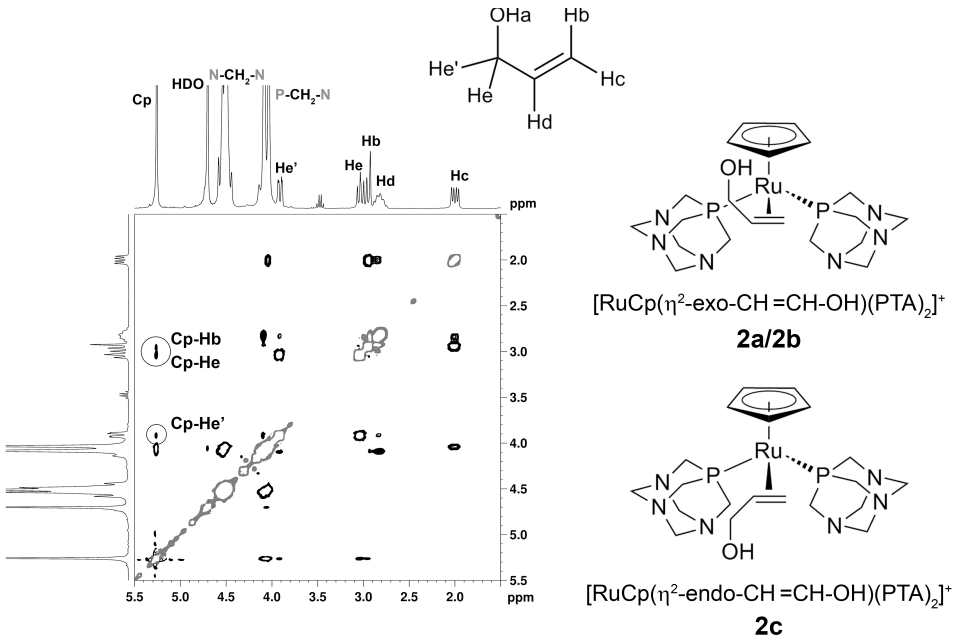

complex **1**, even in dry conditions. ^{1}H and $^{31}P\{^{1}H\}$ NMR spectroscopy show that the same intermediate forms in the three solvents and it is stable enough for its characterisation. This intermediate was synthesised by reaction of **1·CF_3SO_3** with 1-propen-3-ol by using the alcohol itself as solvent (see Experimental section and SI for details). The resulting complex **2·CF_3SO_3** remains stable for days at room temperature and under inert atmosphere, even at high concentration (0.5M) in water. Unfortunately, it was not possible to obtain single crystals of **2·CF_3SO_3**, which was eventually characterised using elemental analysis, IR and NMR spectroscopy. The NMR spectra show that, when dissolved in water, MeOH or 1-propen-3-ol, the complex **2·CF_3SO_3** maintains its structure, irrespective of the solvent. It is important to notice that the highlighted cross peaks in the ^{1}H-^{1}H NOESY spectrum (Figure 1, left) are related to homonuclear spatial correlations be

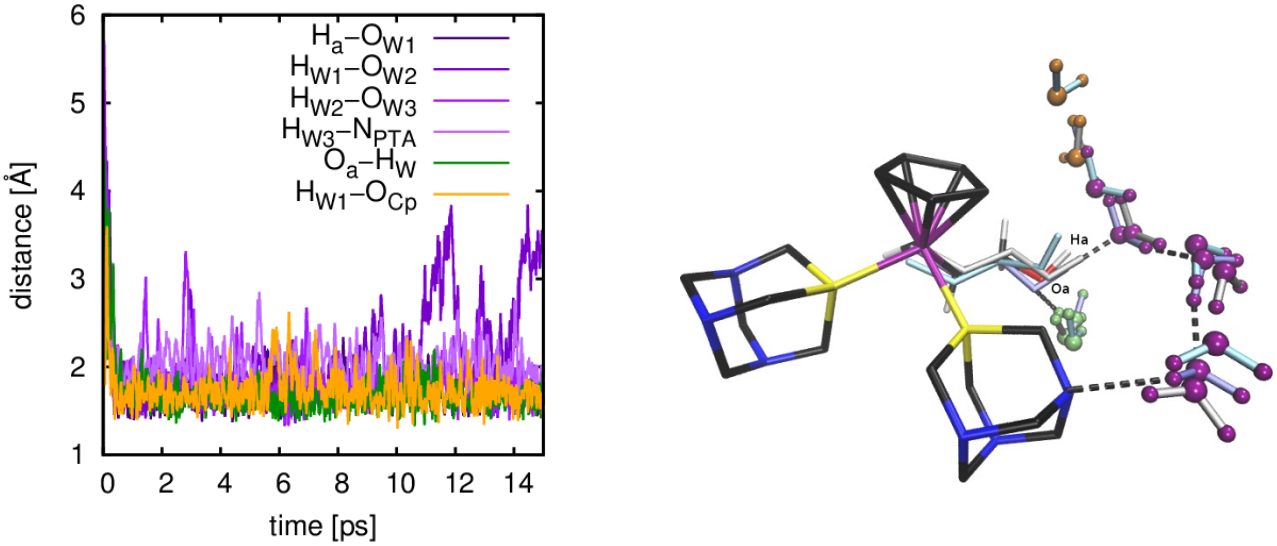

Figure 2. AIMD results for **2a**. Left: Distance evolution during an AIMD simulation for relevant water molecules forming a water chain (purple) and connection to the Cp water network (orange), as well as the water molecule coordinating to the allylic hydroxyl oxygen Oa (green) for **2a**. Right: Overlay of snapshots of **2a** after 6 (violet), 8 (silver) and 10 ps (cyan) including three bridging water molecules (purple spheres), the secondary water coordinating to the Oa (green spheres) and the water molecule linking the water chain to Cp (orange spheres).

tween the α-hydrogens of the allylic alcohol and the Cp hydrogens, and indicate that the exo-η^2-C=C-Ru configuration (**2a**/**2b**, Figure 1, right) is the most probable, as the proximity of these atoms is maintained in this configuration. The hydrogen of the allylic hydroxyl group (Ha) bonded to the allylic-oxygen (Oa) was not observed in the NMR (Figure 1).

NMR maps provide structural information concerning the most probable intermediate, but they cannot be used to obtain details of how water molecules are arranged in the vicinity of the cation **2** and how they interact with it, nor to determine whether they are responsible for the observed conformation of this complex. Furthermore, NMR spectroscopy does not provide accurate values for the distances and angles between the different components of the complex or their orientation. AIMD simulations can be used to obtain information on the solvation structure of **2**, but they are limited, in practice, by their inability to span a set of instantaneous configurations sufficient to represent the actual solvent. For this reason, in this work, we explore the combined use of AIMD and neutron scattering experiments to obtain a reliable and robust description of the water molecule arrangement in the vicinity of **2**.

2.2 Ab initio molecular dynamics (AIMD) simulations. Starting from the structural information obtained from NOESY/NMR for the conformation of **2**, we set up periodic AIMD simulations (see Method section for details) in which both the solute **2** and a number of water molecules sufficient to screen **2** from surrounding solute molecules are explicitly treated quantum-mechanically.

Four different conformational isomers of **2** were selected for gas phase pre-optimisations with DFT: two η^2-exo-allyl-isomers **2a** and **2b** that differ only in an increased dihedral angle of the alkyl C-C bond for **2b** causing the allylic hydroxyl group facing away from the complex, the η^2-endo-C=C-Ru-isomer **2c** and the O-coordinated isomer **2d** (Scheme 4).

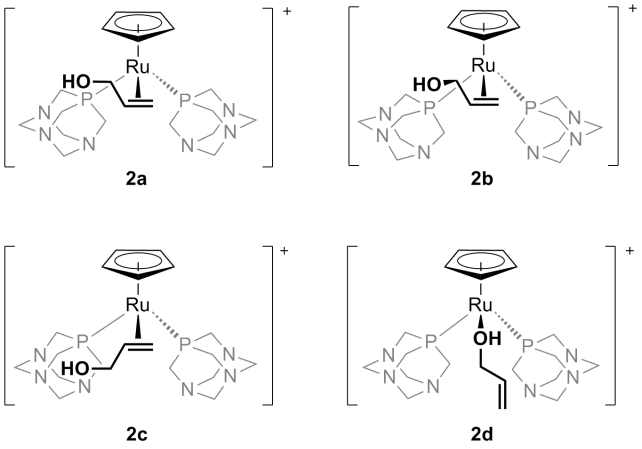

Scheme 4. Calculated possible minimum structures of **2**.

Conformer **2a** is energetically the most stable followed by **2b** (3.7 kcal/mol), **2c** (6.5 kcal/mol) and **2d** (9.6 kcal/mol). In addition to being the least stable, the coordination of conformer **2d** is inconsistent with evidence from the NMR measurements (Figure 1). For this reason we will not consider it further. It should be noted that the gas-phase energy differences between **2a**, **2b** and **2c** are modest, which indicates that the potential energy surface for interconversion is very shallow. This is related to the fact that the isomers differ mainly in the rotational angle around an alkyl C-C bond, which has usually a small rotational barrier. Upon solvation, which is simulated in our approach by surrounding **2** with water molecules within a periodically repeated simulation cell, significant changes from the gas phase optimised structure are observed concerning the allylic hydroxyl orientation at room temperature (see the O-C bond dihedral angle evolution in SI, Figure S14), while the relative orientation of the vinyl group relative to the alcohol moiety does only marginally change with average values of 160.7° for **2a** and 277.1 and 77.4 for **2b** and **2c**, respectively, for the alkyl C-C dihedral angle. This structural change, which marks the transition from a gas-phase to a hydrated complex, occurs within 0.1 ps in our simulations for all three conformers **2a**, **2b** and **2c**. Furthermore, a fast (ca. 200 fs) major structural rearrangement is observed in the water molecule configuration in close vicinity to **2a**. Initially randomly oriented water molecules correlate their trajectories to form a three-membered water chain connecting the hydrogen atom of the allylic-hydroxyl group (Ha) to one of the nitrogen atoms of a PTA ligand (Figure 2, right). This water chain is stable enough to persist for at least 15 ps, with hydrogen oxygen/nitrogen distances predominantly below the hydrogen bond threshold of 2.5 Å. Sporadic minor deviations in the evolution of the latter bond distances occur only by substitution of single waters in direct vicinity of the chain. In addition to this relatively stable phenomenon there are two more water molecules that show peculiar behaviour during the 15 ps simulations: the first molecule is in a locked position coordinating to allylic-oxygen Oa (Figure 2, green spheres) and the second one is linking the first water molecule of the water chain to the previously observed water network around Cp[21] (Figure 2, orange spheres).

Similar to **2a,** the formation of a chain of three water molecules bridging the allyl hydrogen and the PTA nitrogen and one secondary water coordinating to the allyl oxygen can be observed in the simulation of **2b**. However, as the orientation of the substrate's hydroxyl group differs from **2a,** the water chain is not facing directly the Cp ligand in this case. Also, the link to the Cp water network consists of two water molecules in total. Overall, the strength of the interactions leading to the formation of water chains is therefore reduced compared to **2a**. According to our simulations, the time required for stable water chains to form in the **2b** solution is about 30 times larger than for **2a** (SI Figure S15). Further loss in stability can be observed in **2c**. An interconnected network of two four-membered water chains from both the allyl hydrogen and oxygen to the PTA ligand forms only temporarily throughout the simulation. We conclude that, of the three conformations tested, **2a**, once the water chains are formed, shows more consistency in water solution and is less likely to change conformation, and subsequently **2a** plays a more important role in the solution structure than **2b** and **2c**. It is important to stress that this fact is consistent with the findings of the ^{1}H-^{1}H NOESY NMR experiments.

To confirm that the formation of water chains for **2a** is not an artefact of our simulations, we carried out nine further simulations of 2 ps duration with the same starting structure for **2a** and a randomized water solvation box obtained from classical MD simulations at high temperatures followed by a few optimisation steps using the same DFT setup as for the AIMD simulation (for details see Method Section). Although we did not see exactly the same three-membered water chain forming in all cases, water links between the hydroxyl group and the PTA were observed in most of these short AIMD simulations (see Supporting Information Figure S16). While their stability cannot be fully assessed, owing to the short simulation times, their variety and influence on the substrate conformation are interesting: the chain comprises between two and four water molecules and starts from Ha in most cases, but can also link to the PTA ligand from Oa. While the hydroxyl orientation is influenced by the nature of the water chain, the average alkyl C-C dihedral angle, and thus the overall structure, reflect the structure found in the 15 ps simulation of **2a**, with $\theta_{C\text{-}C}$ = 150-162° for water chains from Ha and only deviating slightly ($\theta_{C\text{-}C}$ = 164-175°) from Oa. As the hydroxyl hydrogen Ha is not directly taking part in any of the proposed mechanisms for the isomerisation to the aldehyde, the orientation of the hydroxyl group is not a decisive factor promoting the reaction.

After solvation of **2a** in water and the stabilisation of its substrate conformation at room temperature, we also studied its behaviour at the reactive temperature. For this purpose, we carried out four AIMD simulations at 80˚C for 7.5 ps, starting from the **2a** structure of the room temperature simulation after 7.5 ps (see Supporting Information Figure S17). As expected, the mobility of the water molecules is higher than at room temperature and the water chains overall show more flexibility. In particular, the water-N_{PTA} hydrogen bond shows a tendency to break occasionally, but, as the rest of the water chain remains intact, the periodic formation of the latter is facilitated. A similar behaviour is observed for the Ha-water hydrogen bond. It should however be noted that the breaking of the H-water bond is typically due to the insertion of the water molecule that we previously described as linking the water chain to the Cp water network and remaining fixed at this position (orange in Figure 2) within the three-membered water chain. Thus the overall integrity of the water chain and the link between Ha and PTA is not compromised; it is only extended by one water molecule to a four-membered chain while the conformation of the substrate is conserved (average alkyl C-C dihedral angle between 156.7 and 161.7˚, see Figure S17).

Furthermore we carried out a simulation equivalent to the one of **2a** at room temperature, using methanol, in place of water, as a solvent. In this case, we did not observe the formation of hydrogen bonds linking the substrate hydroxyl group to a PTA ligand, and only single methanol molecules coordinating to the hydroxyl Ha and Oa were found to be present (Supporting Information, Figure S18). Similar to our findings in the simulations of **2a** in water, there is indeed one methanol molecule located between the Cp ring and the methanol molecule coordinated directly to Ha. In methanol, the average alkyl C-C dihedral angle decreases to 140.4˚ and thus leads to a conformation in which the alkyl arm is turned further away from the catalytic Ru centre of the catalyst. Comparing the orientation of the alkyl hydrogen atom that is transferred to the ruthenium atom in the proposed mechanisms (Scheme 3,b), this actually leads to a shorter average Ru-H distance of 3.33 Å with respect to 3.34 Å for **2a** and 3.39 and 3.47 Å for **2b** and **2c**, respectively. However, the hydrogen atom position relative to the rest of the ruthenium complex seems less favourable with respect to the tetrahedral coordination of Ru: the average angles for P_{PTA1}-Ru-H_{alkyl} and P_{PTA2}-Ru-H_{alkyl} for the methanol solvated complex with 83.9˚ and 144.2˚ deviate significantly from the ideal tetrahedral angle of 109˚, while for **2a** (100.3/138.1˚) and **2b** (100.0/135.5˚) in water the deviation is much smaller and therefore the overlap with a bond forming orbital should be larger. Conformation **2c** ranks far behind with average angles of 59.8 and 100.7˚. This finding is important to clarify the role of water interactions with the solute reactive complex and the formation of the water chains in the catalytic process. The absence of a solvent molecule chain in methanol capable of stabilising a substrate conformation suitable for the reaction to occur is likely to be the main reason why the catalytic isomerisation does not proceed in methanol. The AIMD simulations thus show that water plays a crucial role in the catalytic process by forming water chains of different lengths and character both at room and at reaction (80˚C) temperature, always linking the substrate to a PTA ligand and constraining the substrate in a well-defined

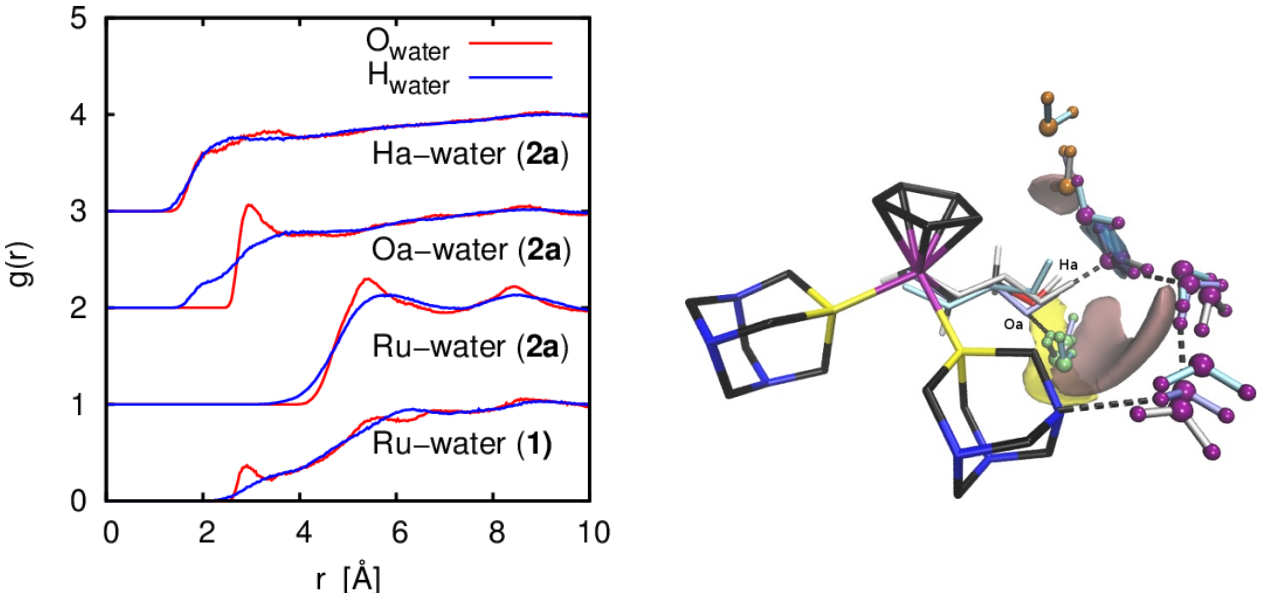

Figure 3. Comparison of AIMD and EPSR results for **2a**. Left: Atom-atom radial distribution function (RDF) for water (O_{water} in red, H_{water} in blue) around the ruthenium atom in catalyst **1** and catalyst with substrate in configuration **2a**. For the latter, also the RDFs for water around the allylic hydroxyl group (Oa, Ha) are shown. Right: Overlay of AIMD snapshots of left panel with EPSR results of right panel. Spatial Density Functions show areas of water probability >50% in the range 1-2 Å (blue), >25% at 2.7-3.5 Å (pink), and >15% at 3.5-4.5 Å (yellow) distance from Ha.

conformation in the vicinity of the catalytic ruthenium centre. The fact that the reaction occurs, experimentally, at 80°C suggests that the substrate conformation in the complex in water is adequate for the isomerisation process to occur, but higher energies are required. A detailed study of the mechanism of the Ru-catalysed isomerisation following the formation of the substrate-catalyst reactive complex is in progress and will be presented elsewhere.

2.3 Neutron scattering experiments and EPSR simulations. Total neutron scattering experiments were performed for **1**·CF_3SO_3 and **2**·CF_3SO_3 on the SANDALS instrument at the ISIS Neutron and Muon Source. This technique, enhanced by hydrogen/deuterium substitution, provides information concerning the positions of hydrogen atoms in solution, and therefore it makes it possible to obtain information concerning hydrogen bonds in water. The resulting neutron datasets were used to constrain an atomistic EPSR simulation (see Experimental Details section). Four simulation boxes were considered: complex **1** with geometry optimised in gas phase using DFT and **2** in configurations **2a**, **2b** and **2c** from the representative snapshots obtained from the AIMD simulations in water solution. From the EPSR simulations, an atomic site-site correlation function can be extracted, either spherically averaged (Radial Distribution Function (RDF), see Figure 3, left) or as a three-dimensional reconstruction (Spatial Density Function (SDF), Figure 3 right).

A well-defined peak in the **1**-Ru–Ow RDF indicates the presence of one water molecule at approximately 3 Å from the Ru atom. An inspection of the corresponding SDF (SI Figure S22) in this distance range shows that this water molecule is bound to the Ru centre, consistent with Ru-OH_2 bond length found in the crystal structure of **1**.[14] In all four simulations, the water molecules in the vicinity of the ruthenium atom have the highest probability at distances between 5 Å and 6 Å, which is more pronounced when the 1-propen-3-ol is bonded to the metal (shown for **2a** in Figure 3) than in **1.** This indicates that **2** has a more pronounced tendency to influence the solvent distribution in its vicinity. The Oa–O_{water} RDF shows a sharp peak at ca. 3.5 Å and the Oa–H_{water} RDF has well defined features at shorter distances, which indicates that a water molecule is bonded to the allylic-Oa through a hydrogen bond. The RDF for Ha–O_{water} distance presents a double peaked structure: the peak below 3 Å is consistent with a water molecule bonded to the hydroxyl hydrogen (Oa–Ha···O_{water}) whilst the peak between 3 Å and 4 Å suggests that one or more water molecules are weakly associated with the complex, but they remain at larger distances. The g(r) peak locations are in good agreement with those obtained from the AIMD simulation (for **2a** in Supporting Information Figure S19), although the simulation peaks are sharper, especially in close vicinity to Oa and Ha. This may be due to the smaller set of configurations sampled by the AIMD simulations compared to the EPSR runs. Furthermore it should be noted that the use GGA functionals in DFT tend to overestimate the interactions between water molecules. It is important to point out that the orientation of the water molecule closest to Ha is not determined by simple dipole-dipole interactions, as indicated by the essentially flat RDF for Ha–H_{water}. This complex structure therefore points to an ordering of the water molecules that is not solely determined by the presence of the Oa-Ha dipole. In order to further investigate this possible water ordering, the SDFs have been extracted for selected radial slices at 1-2 Å (blue), 2.7-3.5 Å (pink) and 3.5-

4.5 Å (yellow), and displayed for **2a** in Figure 3 right side. For the first slice in the range between 1 Å and 2 Å we observe very localised density in the prolongation of the Oa–Ha axis for all conformations **2a-c** (for data on **2b** and **2c** see SI Figures S26 and S27). This represents a water molecule bonded through its H atom to the allylic-Oa atom (purple spheres in Figure 3), which was also observed in the AIMD simulations for all conformers. The second radial slice at 2.7-3.5 Å (pink) shows a more localised distribution of peaks for **2a**, with a larger area between the hydroxyl and the PTA and a smaller one between the allylic-hydroxyl and the Cp. Another smaller high-density area is observed in the SDF between the SDF at 1-2 Å (blue, position of first water chain link) and the Cp ligand. The superposition of the spatial densities obtained by EPSR analysis with snapshots from the AIMD simulation of **2a** (Figure 3, right) shows striking agreement. In addition to the above mentioned first water chain link in close proximity to Ha, also the water molecule appearing in the AIMD simulations in a relatively stable position between the latter and the Cp ring (orange spheres) is well accounted for by the EPSR spatial density (pink). The second water molecule in the water chain, which was observed bonded to the Oa (green spheres) in the AIMD simulations, is well represented by the localised SDF features in the vicinity of the Cp ligand. The remaining spatial slice at 3.5-4.5 Å also shows distinct localisation near Oa. This confirms the stability of the hydrogen bonds between the allylic-OH and water molecules and the existence of sizable interactions of the latter with surrounding water molecules. Although we did only analyse this specific case of a three-membered water chain for **2a** in detail, it should be noted that also the alternative water chains composed of two to four water molecules that we have observed in the 2 ps AIMD simulations are consistent with this picture. In particular, for those simulations in which the O-C dihedral angle does not undergo a conformational change, the structures of the complex are very close to the one considered in the EPSR simulations. In all these AIMD water distributions, a water molecule is closely coordinating Ha and Oa and all these chains extend towards the PTA ligands and thus to areas where the EPSR shows water abundance (2.7-3.5 Å (pink) and 3.5-4.5 Å (yellow) in Figure 3).

In contrast to conformation **2a**, much more delocalised spatial densities for the same radial slices are obtained for conformations **2b** and **2c** (SI Figures S26 and S27). Overall EPSR results for **2b** and **2c** show a homogeneous distribution of water molecules around allylic-hydrogen atom Ha. Although the water chains and single interacting water molecules observed in the AIMD simulations for **2b** and **2c** do overlap in part with the SDF obtained from EPSR, both the periodic hydrogen bond breaking within the chains observed in the AIMD and the delocalisation of the EPSR spatial densities indicate a much higher system flexibility for these conformers.

The excellent agreement of our AIMD results and the EPSR simulations for **2a** confirms that water molecules occupy relatively stable positions around the solute over time-scales sufficient for detection with neutron techniques. As the EPSR results represent experimental neutron scattering data, this is also a strong indication that conformation **2a** plays a dominant role in the reaction mixture.

3. CONCLUSION

In this work, we have presented a model of how solute-water interactions affect the stability, and potentially the overall catalytic activity of complex **1** in the isomerization of 1-propen-3-ol. Our work uses a combination of experimental techniques (NMR and total neutron scattering) and computational approaches (AIMD and EPSR simulations) to obtain detailed microscopic insight into the solvation structure of the observed intermediate species in this catalytic reaction, the complex $[RuCp(\eta^2\text{-}CH_2\text{=}CH\text{-}CH_2\text{-}OH)(PTA)_2]^+$ (**2**). We have confirmed that the coordination of the allyl alcohol is consistent with an exo-η^2-C=C-Ru configuration after the replacement of a vacant water site on the metal centre. Analysis of the neutron data on the water solution of **2** with AIMD simulations indicate that changes in the hydroxyl group orientation of the reactive complex occur upon solvation, relative to the hypothetical micro-solvated gas phase species. A peculiarly directional interaction of the most stable isomer of **2** with surrounding water molecules leads to the formation of stable chains of water molecules bridging the allyl-hydroxyl hydrogen (Ha) or oxygen (Oa) with a N_{PTA}. These structures form from different water distributions and can persist when propagated for 15 ps according to our AIMD results. The formation of water chains is linked to the stabilisation of only one among the set of potential isomers of **2** identified in gas-phase DFT calculations, the isomer **2a**. For all other isomers, water chains appear as transient species. The existence of water chains linked to **2** is supported by the strong similarity between the water molecule positions predicted using neutron scattering and the AIMD simulations (Figure 3, right). The existence of stable closed chains of water molecules and their influence on reactivity have recently been put forward based on AIMD simulations, e.g. in the context of water oxidation reactions.[21] This work presents the first experimental evidence for the existence of these species in water solutions and of their involvement in chemical reactivity.

We note that the catalytic isomerization of 1-propen-3-ol by **1** in water has a very low conversion, even at temperature as high as 80 ºC (ca. 12%), in contrast to reactions carried out on longer linear allylic alcohols in which full conversion was obtained in a few hours.[14] The observed yield in water is however significantly larger than in dry MeOH and 1-propen-3-ol as solvent. Although overall flexibility of the water chains increases when continuing the simulations at reactive temperature, the water chain motive and substrate conformation are conserved. This differs when the simulation is carried out in methanol, where no hydrogen bond network linking the substrate to the PTA ligand is formed and the substrate conformation changes rotating around the alkyl C-C bond, which leads to a potentially less favourable position for isomerisation for the alkyl hydrogen atom with respect to

the catalytic ruthenium centre. This indicates that the disposition for the catalytic reaction of **2** is affected in a very characteristic way by the water environment, and that it is the solvation process as a whole (as described e.g. in our AIMD simulations on water solutions), rather than the simple coordination of water molecules (as in gas-phase micro-solvated models of **2**), that determines the chemical behaviour of **2** in water. According to our results, water as a reaction medium is capable not only to favour the most reactive isomer of **2** in the early stages of the isomerisation, but might also influence and further enhance the reactivity of the complex. Further work combining NMR, AIMD and neutron scattering is in progress to determine the role of water molecules in promoting the isomerization reactions catalysed by **1**, with the aim to gain a more complete understanding solute-solvent interactions in this catalytic reaction in a variety of working environments and to obtain additional information on the catalytic isomerization of allylic alcohols larger than 1-propen-3-ol lineal in water with **1**.

Our study demonstrates that a combination of AIMD simulations and total neutron scattering is a powerful tool for identifying unusual solvation motifs for complex solutes and for studying the role of individual water molecules in the stabilisation of reaction intermediates. This is of particular importance as aqueous solutions often pose a challenge to many classical analytical methods. Our approach provides a useful tool for characterising the conformation of key intermediates in catalytic reactions in water solution, as well as for studying how solute-solvent interactions affect the reaction outcomes, both in water and in non-aqueous solvents.

5. EXPERIMENTAL DETAILS

Catalysis. Catalytic isomerization of 1-propen-3-ol with **1·CF_3SO_3·3.5H_2O** and **1·CF_3SO_3** in water, MeOH and 1-propen-3-ol was carried out under nitrogen in six 5 mm NMR tubes: three containing as catalyst **1·CF_3SO_3·3.5H_2O** (5 mg, 0.007 mmol), which was obtained as indicated in ref 14, and in the other three the dry **1·CF_3SO_3** (4.5 mg, 0.007 mmol) dissolved in 0.5 mL of 1-propen-3-ol, H_2O and MeOH. Into the tubes with H_2O and MeOH also 1-propen-3-ol (48 µL, 0.7 mmol) was added. The six tubes were kept at room temperature and 80 ºC for 2 days, observing the conversion only at 80 ˚C in water (12.1(6) %). In dry MeOH and 1-propen-3-ol the conversion was 1.5(5) % and 1.1(5) %, respectively.

Synthesis of 2·CF_3SO_3. Under nitrogen complex **1·CF_3SO_3·3.5H_2O** (3 g, 4.2 mmol) was dissolved in 15 mL of deoxygenated 1-propen-3-ol at room temperature. The solution was stirred during 1 h at room temperature and then 10 mL of EtOH and 100 mL of Et_2O were added. The resulting precipitated white powder was filtered, washed with Et_2O (3 x 30 mL) and dried under vacuum. Yield: 2.6 gr (90%). S_{25,H_2O} (g/mL): 1.3. Elemental analysis for powder sample $C_{21}H_{35}F_3N_6O_4P_2RuS$ (687.6 g·mol^{-1}): Found C: 36.48, H 5.31, N 12.35; calcd. C 36.68, H 5.13, N 12.22. IR (KBr, cm^{-1}): 2922 (m); 1448 (m), 1410 (m), 1280 (s), 1247 (s), 1222 (m), 1154 (m), 1106 (m), 1031 (s), 1016 (m), 976 (s), 949 (m), 895 (w), 846 (w), 812 (m), 745 (m), 639 (m), 581 (m), 517 (w), 477 (w), 451 (w), 432 (w). ^{1}H NMR (300.13 MHz, 22 °C, D_2O): δ 1.95-2.08 (m, 1H, H_c), 2.73-2.90 (m, 1H, H_d), 2.91-2.98 (m, 1H, H_b), 2.99-3.10 (m, 1H, H_e), 3.87-3.97 (m, 1H, $H_{e'}$), 3.99-4.20 (m, PCH_2N, 12 H), 4.41-4.64 (m, NCH_2N, 12 H), 5.27 (s, Cp, 5H). ^{13}C{^{1}H} RMN (75.467 MHz, 22 °C, D_2O): δ 34.3 (d, $^2J_{CP}$ = 4.9 Hz,), 53.8-54.3 (dd, $^1J_{CP}$ = 18.4 Hz, $^3J_{CP}$ = 1.9 Hz, NCH_2P), 54.4-54.8 (dd, $^1J_{CP}$ = 17.7 Hz, $^3J_{CP}$ = 2.1 Hz, NCH_2P), 55.4 (d, $^2J_{CP}$ = 4.4 Hz,), 67.2 (s,), 70.5 (d, $^3J_{CP}$ = 1.1 Hz, NCH_2N), 70.5 (d, $^3J_{CP}$ = 1.1 Hz, NCH_2N), 85.6 (s, Cp), 113.3-126.0 (q, $^1J_{CF}$ = 318.0 Hz, CF_3SO_3) ^{31}P{^{1}H} NMR (121.49 MHz, 22 °C, D_2O): δ -21.50 (d, $^2J_{PP}$ = 42.3 Hz, P1), -23.40 (d, $^2J_{PP}$ = 42.3 Hz, P2). (Further details in Supporting Information)

AIMD Simulations. Geometries were optimised applying density functional theory (DFT) at the B3LYP[22,23]/def2-TZVPP[24] level of theory with the NWChem6.6 program package[25] and equivalent to our AIMD simulations (see below). The effective core potential def2-ecp was applied to atom Ru. A water/methanol box of 79 water/methanol molecules was added to the molecules with the Solvate Plugin in VMD 1.9.2. The box dimensions were chosen to correspond a water density of 1 g/cm3 added to the volume of the molecule as determined with the program Mol_Volume[26] using van der Waals radii[27]. Ab initio molecular dynamic simulations (AIMD) were then performed using the hybrid Gaussian/plane-wave[28] package CP2K Quickstep[29,30] version 2.7. The PBE functional, a standard double-ζ VB basis sets and Goedecker-Teter-Hutter pseudopotentials[31] were used for all atomic species. A cutoff of 310 Ry was used in the plane-wave expansion. Atomic positions were propagated using Born-Oppenheimer dynamics[32] in an NVT ensemble and with a time-step of 0.5 fs under periodic boundary conditions for 2, 7.5 or 15 ps. The simulation temperature was set to 298/353 K and was controlled through a Nosé-Hoover thermostat. Randomisation of the water box was achieved by classical molecular dynamics simulation at 900 K for 2.5 ps with constrained complex structure using the DLPOLY 2 code,[33] followed by 30-50 DFT optimisation steps equivalent to the method used in the AIMD simulation. Visualisation of results was done using VMD – Visual Molecular Dynamics[34].

Neutron diffraction and EPSR simulations. The neutron experiment has been performed on the SANDALS diffractometer at the ISIS Neutron and Muon source (UK), a diffractometer optimised for hydrogen containing liquid and amorphous samples. Complex **2** has been dissolved at 0.5M concentration in H_2O, D_2O and an equimolar mixture of the two (labelled HDO). The three solutions have been transferred in flat TiZr alloy cans (sample thickness 1mm) and measured at 25°C under a white beam. The neutron data have been carefully corrected for detector efficiency, attenuation, multiple scattering and inelastic scattering using well-established methods[35]. Computational models of the system have been obtained through Empirical Potential Structure Re-

finement (EPSR)[36]. The algorithm is based on a classical Monte Carlo simulation of the molecular system under study at fixed concentration and density. It employs an iterative algorithm aimed at building a three dimensional model consistent with the scattering data. The simulation box contains 20 molecules of **2** (**2a**, **2b** and **2c** have been tested in three different simulation boxes), 20 triflate anions and 2200 water molecules. The geometry and Coulomb partial charges of **2a**, **2b** and **2c** have been determined from representative snapshots from AIMD simulations. For the water molecule a classic SPC/E model[37] has been adopted.

ASSOCIATED CONTENT

Supporting Information. Details on synthesis, NMR spectra, AIMD determinations and EPSR simulations. This material is available free of charge via the Internet at http://pubs.acs.org

AUTHOR INFORMATION

Corresponding Author

*E-mail: romerosa@ual.es

ACKNOWLEDGMENT

AR thanks "Modalidad A of Estancias de profesores e investigadores senior en centros extranjeros, incluido el Programa 'Salvador de Madariaga'," (ref: PRX16/00442; Ministerio de Educación, Cultura y Deportes) for supporting his 6-month stay at STFC Rutherford Appleton Laboratory (UK). We thank the European Commission FEDER program for cofinancing the projects CTQ2015-67384-R (MINECO), the Junta de Andalucía PAI-research group FQM-317 and COST Action CM1302 (WG1, WG2). AR and SI acknowledge the beamtime awarded at the ISIS Neutron and Muon source (RB1300023). NH and LB acknowledge support from the UK HPC Materials Chemistry Consortium (grant EP/L000202) and from the EPSRC Service Level Agreement with STFC Scientific Computing Department.

REFERENCES

(1) Van Der Drift, R. C.; Bouwman, E.; Drent, E. *Journal of Organometallic Chemistry*. 2002, pp 1–24.

(2) Uma, R.; Crévisy, C.; Grée, R. *Chem. Rev.* **2003**, *103* (1), 27–51.

(3) Cadierno, V.; Crochet, P.; Gimeno, J. *Synlett*. 2008, pp 1105–1124.

(4) Ahlsten, N.; Bartoszewicz, A.; Martín-Matute, B. *Dalt. Trans.* **2012**, *41* (6), 1660–1670.

(5) Mendoza, Z.; Lorenzo-Luis, P.; Serrano-Ruiz, M.; Martín-Batista, E.; Padrón, J. M.; Scalambra, F.; Romerosa, A. *Inorg. Chem.* **2016**, *55* (16).

(6) Hajji, L.; Saraiba-Bello, C.; Romerosa, A.; Segovia-Torrente, G.; Serrano-Ruiz, M.; Bergamini, P.; Canella, A. *Inorg. Chem.* **2011**, *50* (3), 873–882.

(7) Ríos-Luci, C.; León, L. G.; Mena-Cruz, A.; Pérez-Roth, E.; Lorenzo-Luis, P.; Romerosa, A.; Padrón, J. M. *Bioorg. Med. Chem. Lett.* **2011**, *21* (15), 4568–4571.

(8) Scalambra, F.; Serrano-Ruiz, M.; Nahim-Granados, S.; Romerosa, A. *Eur. J. Inorg. Chem.* **2016**, *2016* (10), 1528–1540.

(9) Campos-Malpartida, T.; Fekete, M.; Joó, F.; Kathó, Á.; Romerosa, A.; Saoud, M.; Wojtków, W. *J. Organomet. Chem.* **2008**, *693* (3), 468–474.

(10) Bolaño, S.; Gonsalvi, L.; Zanobini, F.; Vizza, F.; Bertolasi, V.; Romerosa, A.; Peruzzini, M. *J. Mol. Catal. A Chem.* **2004**, *224* (1–2), 61–70.

(11) Saoud, M.; Romerosa, A.; Peruzzini, M. *Organometallics* **2008**, *19* (20), 4005–4007.

(12) González, B.; Lorenzo-Luis, P.; Serrano-Ruiz, M.; Papp, É.; Fekete, M.; Csépke, K.; Osz, K.; Kathó, Á.; Joó, F.; Romerosa, A. *J. Mol. Catal. A Chem.* **2010**, *326* (1–2), 15–20.

(13) Serrano-Ruiz, M.; Lorenzo-Luis, P.; Romerosa, A.; Mena-Cruz, A. *Dalt. Trans.* **2013**, *42* (21), 7622.

(14) Scalambra, F.; Serrano-Ruiz, M.; Romerosa, A.; Bergman, R. G.; Raymond, K. N.; Kenneth, N.; Peruzzini, M.; Sava, G.; Bergamo, A.; Romerosa, A. *Dalt. Trans.* **2017**, *46* (18), 5864–5871.

(15) Cadierno, V.; García-Garrido, S. E.; Gimeno, J.; Varela-Álvarez, A.; Sordo, J. A. *J. Am. Chem. Soc.* **2006**, *128* (4), 1360–1370.

(16) Bellarosa, L.; Díez, J.; Gimeno, J.; Lledós, A.; Suárez, F. J.; Ujaque, G.; Vicent, C. *Chem. - A Eur. J.* **2012**, *18* (25), 7749–7765.

(17) Díez, J.; Gimeno, J.; Lledós, A.; Suárez, F. J.; Vicent, C. *ACS Catal.* **2012**, *2* (10), 2087–2099.

(18) Batuecas, M.; Esteruelas, M. A.; García-Yebra, C.; Oñate, E. *Organometallics* **2010**, *29* (9), 2166–2175.

(19) Lorenzo-Luis, P.; Romerosa, A.; Serrano-Ruiz, M. *ACS Catalysis*. 2012, pp 1079–1086.

(20) Serrano-Ruiz, M.; Imberti, S.; Bernasconi, L.; Jadagayeva, N.; Scalambra, F.; Romerosa, A. *Chem. Commun.* **2014**, *50* (78), 11587–11590.

(21) Bernasconi, L.; Kazaryan, A.; Belanzoni, P.; Baerends, E. J. *ACS Catal.* **2017**, *7* (6), 4018–4025.

(22) Becke, A. D. *J. Chem. Phys.* **1993**, *98* (7), 5648.

(23) Lee, C.; Yang, W.; Parr, R. G. *Phys. Rev. B* **1988**, *37* (2), 785–789.

(24) Weigend, F.; Ahlrichs, R.; Peterson, K. A.; Dunning, T. H.; Pitzer, R. M.; Bergner, A. *Phys. Chem. Chem. Phys.* **2005**, *7* (18), 3297.

(25) Valiev, M.; Bylaska, E. J.; Govind, N.; Kowalski, K.; Straatsma, T. P.; Van Dam, H. J. J.; Wang, D.; Nieplocha, J.; Apra, E.; Windus, T. L.; de Jong, W. A. *Comput. Phys. Commun.* **2010**, *181* (9), 1477–1489.

(26) Balaeff, A. Mol_Volume - Calculate macromolecular volume http://www.ks.uiuc.edu/Development/MDTools/molvolume/ (accessed Aug 2, 2017).

(27) Mantina, M.; Chamberlin, A. C.; Valero, R.; Cramer, C. J.; Truhlar, D. G. *J. Phys. Chem. A* **2009**, *113* (19), 5806–5812.

(28) Lippert, B. G.; Parrinello, J. H. and M. *Mol. Phys.* **1997**, *92* (3), 477–488.

(29) Vandevondele, J.; Krack, M.; Mohamed, F.; Parrinello, M.; Chassaing, T.; Hutter, J. *Comput. Phys. Commun.* **2005**, *167* (2), 103–128.

(30) Quickstep. quickstep [CP2K Open Source Molecular Dynamics] https://www.cp2k.org/quickstep (accessed Aug 2, 2017).

(31) Goedecker, S.; Teter, M.; Hutter, J. *Phys. Rev. B* **1996**, *54* (3), 1703–1710.

(32) Marx, D.; Hutter, J. *Publication Series of the John von Neumann Institute for Computing (NIC) NIC Series*; 2000; Vol. 1.

(33) Smith, W.; Forester, T. R. *J. Mol. Graph.* **1996**, *14* (3), 136–141.

(34) Humphrey, W.; Dalke, A.; Schulten, K. *J. Mol. Graph.* **1996**, *14* (1), 33–38.

(35) Soper, A. *RAL Tech. Rep.* **2011**, No. July, RAL-TR-2011-013.

(36) Soper, A. K. *RAL Tech. Rep.* **2011**, No. May, RAL-TR-2011-012.
(37) Berendsen, H. J. C.; Grigera, J. R.; Straatsma, T. P. *J. Phys. Chem.* **1987**, *91* (24), 6269–6271.